Energy Materials

Supplementary Materials

Enhanced oxygen evolution of FeNiMoRuZn sulfide through Zn-enabled multiscale stabilization

Shasha Gao[1,2], Jinteng Guan[1], Hongmei Chen[1], Feifei Mao[1,3], Jiacong Lei[2], Dong Guo[2,*], Yang Gao[4,*], Yingbin Li[1,*], Gonglei Shao[2,*]

[1]Key Laboratory of Microelectronics and Energy of Henan Province, Department of Physics and Electronic Engineering, Xinyang Normal University, Xinyang 464000, Henan, China.
[2]Interdisciplinary Research Center for Sustainable Energy Science and Engineering (IRC4SE[2]), School of Chemical Engineering, Zhengzhou University, Zhengzhou 450001, Henan, China.
[3]Department of System Semiconductor Engineering, Cheongju University, Cheongju 28503, South Korea.
[4]Collaborative Innovation Center, Henan Academy of Sciences, Zhengzhou 450046, Henan, China.

[*]**Correspondence to:** Prof. Gonglei Shao, Dr. Dong Guo, Interdisciplinary Research Center for Sustainable Energy Science and Engineering (IRC4SE[2]), School of Chemical Engineering, Zhengzhou University, Zhengzhou 450001, Henan, China. E-mail: shaogonglei@zzu.edu.cn; guodong@gs.zzu.edu.cn; Prof. Yingbin Li, Key Laboratory of Microelectronics and Energy of Henan Province, Department of Physics and Electronic Engineering, Xinyang Normal University, Xinyang 464000, Henan, China. E-mail: liyingbin@xynu.edu.cn; Dr. Yang Gao, Collaborative Innovation Center, Henan Academy of Sciences, Zhengzhou 450046, Henan, China. E-mail: yanggao@hnas.ac.cn

EXPERIMENTAL

Characterization

X-ray diffraction (XRD) patterns were recorded on a Rigaku Ultima IV diffractometer (Rigaku Corporation, Japan) using Cu Kα radiation (λ = 1.5406 Å) operating at 40 kV and 40 mA. The data were collected in the 2θ range of 5° to 80° with a scanning speed of 5° min^{-1}. Transmission electron microscopy (TEM) images and energy dispersive X-ray spectroscopy (EDS) mappings were acquired using a Tecnai G2 F20 (FEI Company, USA) microscope equipped with a probe corrector and a monochromator, operating at an acceleration voltage of 200 kV. Nitrogen adsorption–desorption isotherms were measured at 77 K using a Micromeritics ASAP 2460 analyzer (Micromeritics Instrument Corporation, USA), and the pore size distribution was calculated using the DFT method. X-ray photoelectron spectroscopy (XPS) measurements were performed on a Thermo Fisher Scientific K-Alpha spectrometer (Thermo Fisher Scientific, USA) using a monochromated Al Kα X-ray source with a spot size of 400 μm. The binding energies were calibrated using the adventitious C1s peak at 284.8 eV. Fourier transform infrared (FTIR) spectra were recorded on a Bruker INVENIO spectrometer (Bruker Optics GmbH, Germany) with a resolution of 2 cm^{-1} in the spectral range of 4000–400 cm^{-1}. The elemental composition of the catalysts was determined by inductively coupled plasma optical emission spectroscopy (ICP-OES) on Agilent 730 instrument (Agilent Technologies, USA). Raman spectra were recorded on a XploRA PLUS spectrometer (Horiba Scientific, France) with a 532 nm laser excitation.

In-situ FTIR measurements

In-situ FTIR spectra were collected using a three-electrode spectroelectrochemical cell (Bruker INVENIO FTIR spectrometer) with a spectral resolution of 2 cm^{-1}. The working electrode was prepared by depositing the catalyst onto carbon paper. A platinum wire served as the counter electrode, and a Ag/AgCl electrode was used as the reference electrode. The working electrode was fabricated as follows: a homogeneous ink containing 2 mg of catalyst, 40 μL of Nafion solution, and 960 μL of ethanol was drop-

cast onto the carbon paper and subsequently dried under ambient conditions. The electrolyte was 1.0 M KOH. Potential-dependent spectra were collected from 1.0 to 1.8 V vs. RHE, and the electrode was held at each potential for 60 s prior to spectral acquisition. During the measurements, the electrolyte was circulated at a flow rate of 30 mL min^{-1} to remove visible oxygen bubbles and avoid optical interference. All measurements for M_4Zn-S and M_4-S were performed under identical conditions to ensure consistency.

The mechanism for OER

The preferred mechanism for the AEM-OER involves a four-electron pathway, which proceeds through the following elementary steps:

$OH^- + * \rightarrow MOH + e^-$

$MOH + OH^- \rightarrow MO + H_2O + e^-$

$MO + OH^- \rightarrow MOOH + e^-$

$MOOH + OH^- \rightarrow M + O_2 + e^- + H_2O$

The preferred mechanism for the LOM-OER involves a four-electron pathway, which proceeds through the following elementary steps:

$O\text{-}M\text{-}O + OH^- \rightarrow O\text{-}M\text{-}O\text{-}OH + e^-$

$O\text{-}M\text{-}O\text{-}OH + OH^- \rightarrow O\text{-}M\text{-}O\text{-}O + H_2O + e^-$

$O\text{-}M\text{-}O\text{-}O \rightarrow O\text{-}M\text{-}Ov + O_2$

$O\text{-}M\text{-}Ov + OH^- \rightarrow O\text{-}M\text{-}OH + H_2O + e^-$

$O\text{-}M\text{-}OH \rightarrow O\text{-}M\text{-}O + H_2O + e^-$

The preferred mechanism for the Copule-OER involves a four-electron pathway, which proceeds through the following elementary steps:

$M\text{-}O\text{-}M\text{-}O + OH^- \rightarrow M\text{-}O\text{-}M\text{-}O\text{-}OH + e^-$

$M\text{-}O\text{-}M\text{-}O\text{-}OH + OH^- \rightarrow M\text{-}O(OH)\text{-}M\text{-}O\text{-}OH + e^-$

$M\text{-}O(OH)\text{-}M\text{-}O\text{-}OH + OH^- \rightarrow M\text{-}O(O)\text{-}M\text{-}O\text{-}OH + H_2O + e^-$

$M\text{-}O(O)\text{-}M\text{-}O\text{-}OH + OH^- \rightarrow M\text{-}O(O)\text{-}M\text{-}O\text{-}O + H_2O + e^-$

$M\text{-}O(O)\text{-}M\text{-}O\text{-}O \rightarrow M\text{-}O\text{-}M\text{-}O + O_2$

Here, * denotes an active chemisorption site.

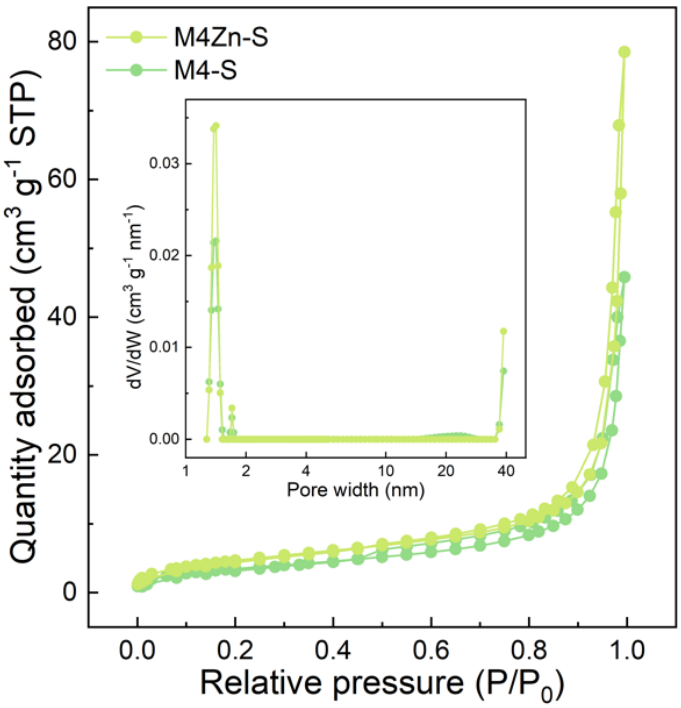

Supplementary Figure S1. BET surface area analysis of M4Zn-S and M4-S.

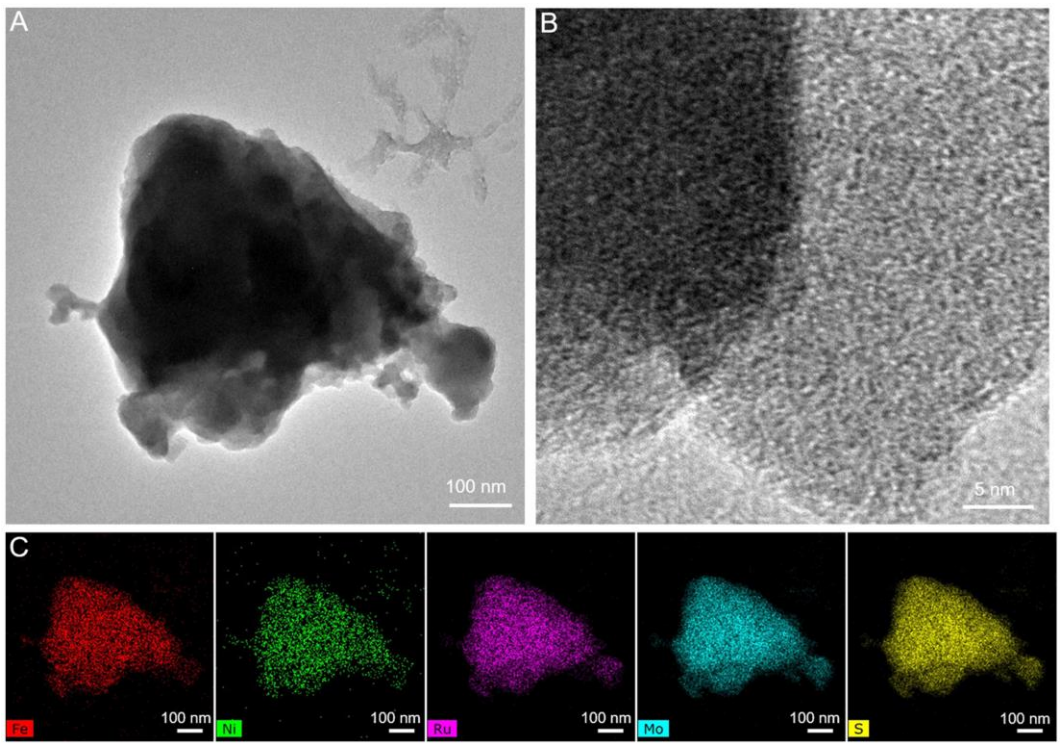

Supplementary Figure S2. TEM (A) and HRTEM (B) images, and TEM elemental mapping (C) of M4-S.

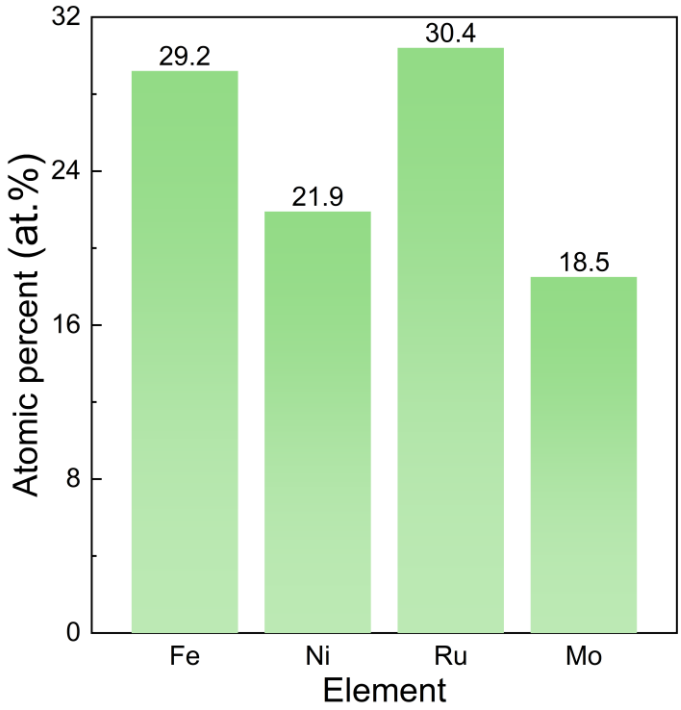

Supplementary Figure S3. Elemental content analysis via ICP of M4-S.

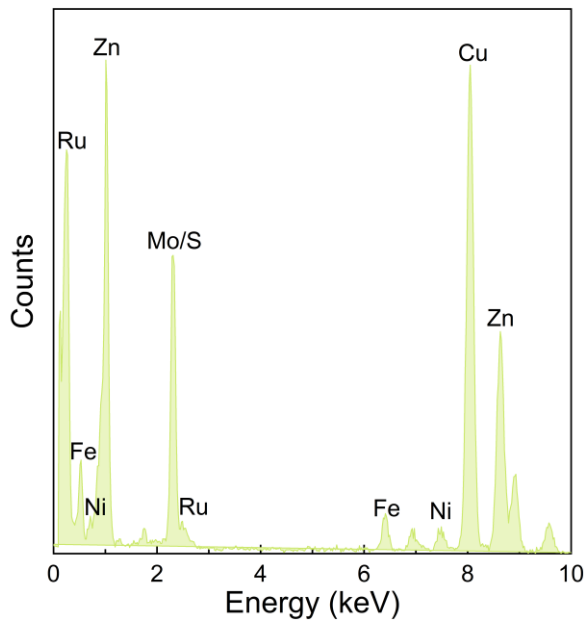

Supplementary Figure S4. Elemental content analysis via TEM-EDS of M4Zn-S. (*Note: The Cu signal arises from the copper supporting grid for TEM-EDS measurement and is not derived from the sample.*)

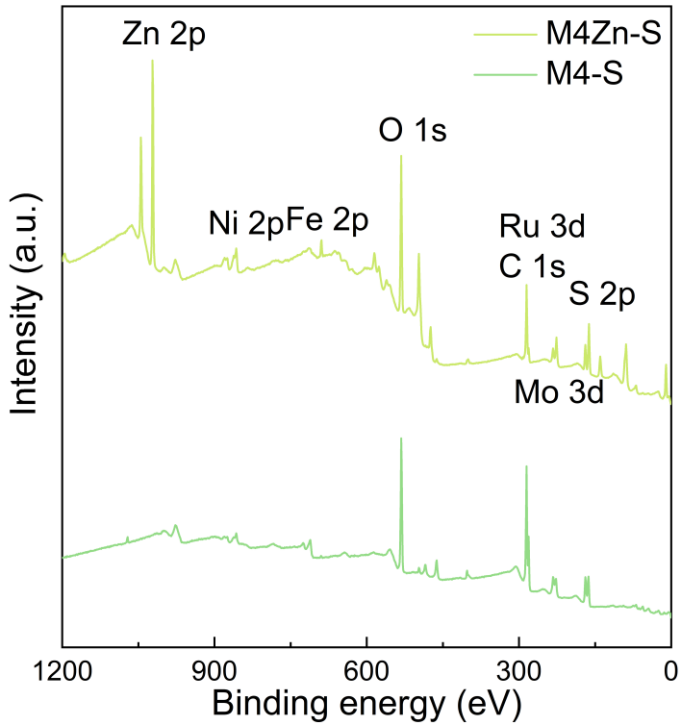

Supplementary Figure S5. XPS survey spectra of M4-S and M4Zn-S.

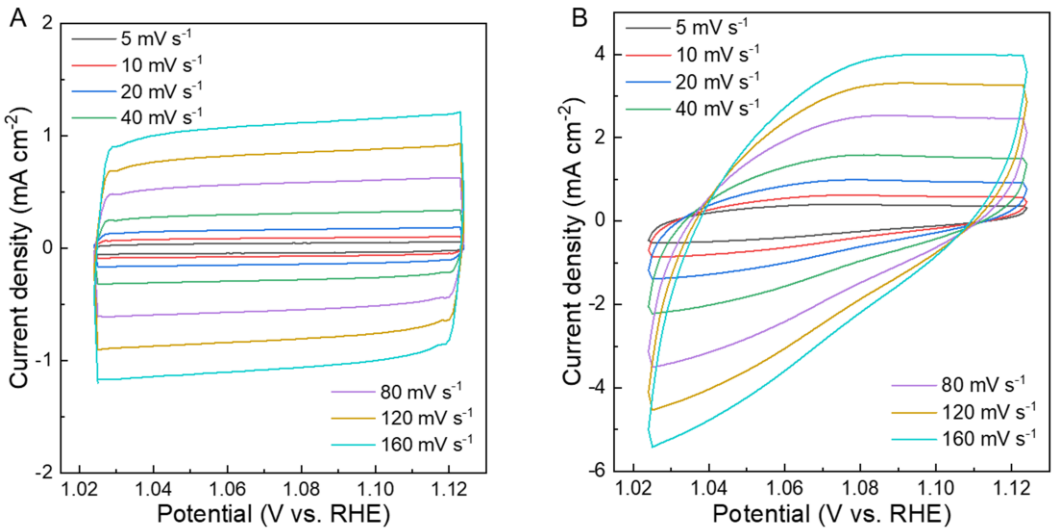

Supplementary Figure S6. Multi-scan-rate CV measurements of (A) M4-S and (B) M4Zn-S.

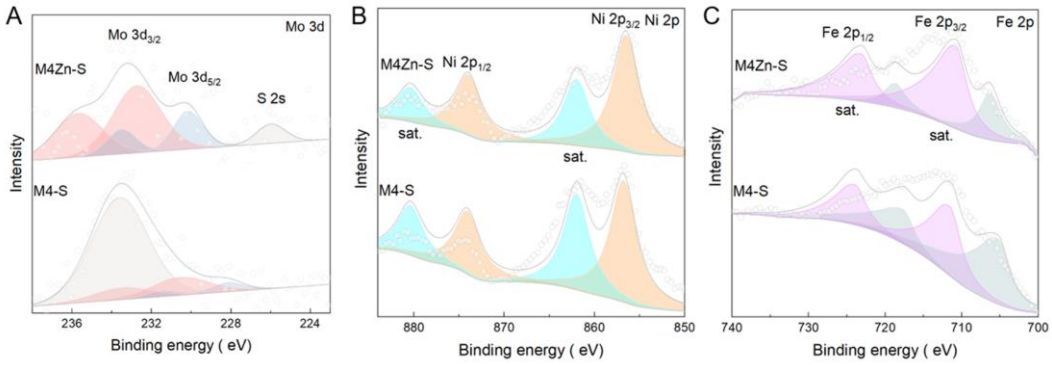

Supplementary Figure S7. XPS spectra of Mo 3d (A), Ni 2p (B) and Fe 2p (C) for M4Zn-S and M4-S after stability testing.

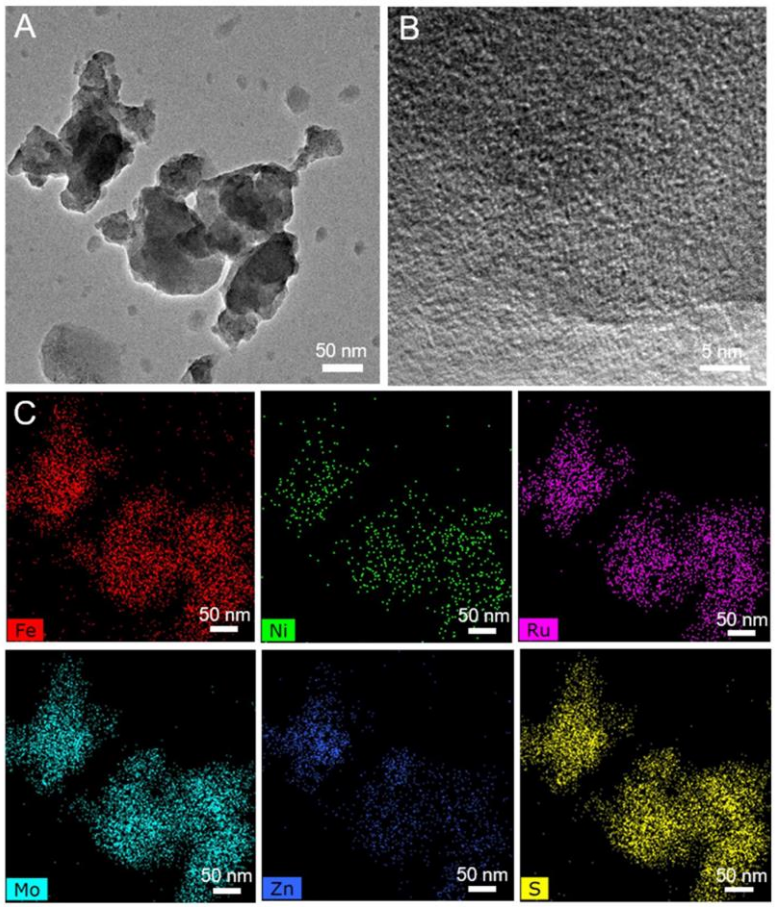

Supplementary Figure S8. TEM (A) and HRTEM (B) images, and TEM elemental mapping (C) of M4Zn-S after AEMWE.

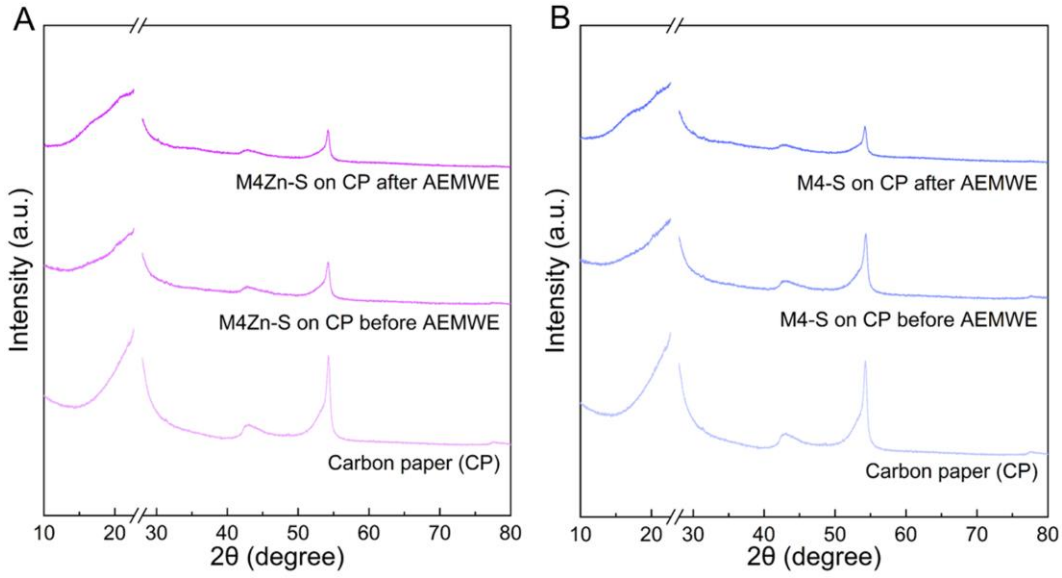

Supplementary Figure S9. XRD patterns of M4Zn-S (A) and M4-S (B).

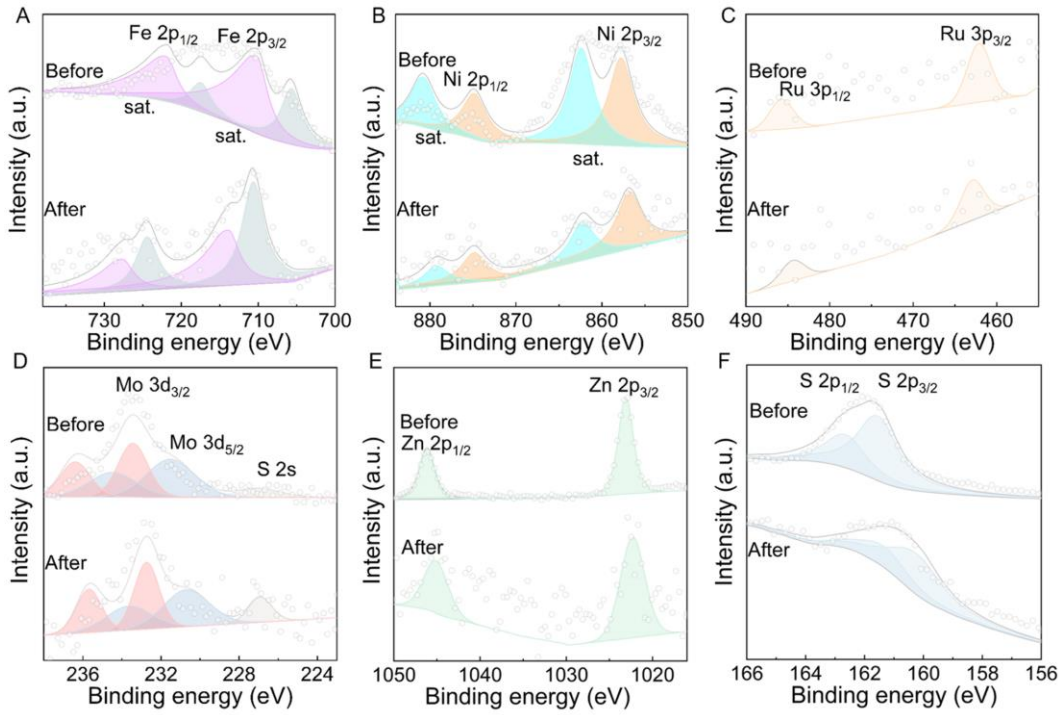

Supplementary Figure S10. XPS spectra including (A) Fe 2p, (B) Ni 2p, (C) Ru 3p, (D) Mo 3d, (E) Zn 2p, and (F) S 2p for M4Zn-S before and after AEMWE.

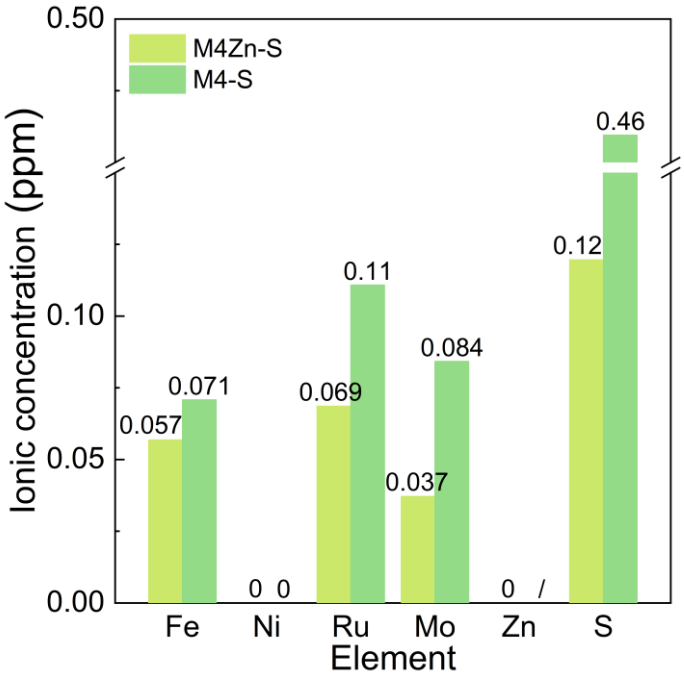

Supplementary Figure S11. The ionic concentration of M4Zn-S and M4-S in electrolyte after AEMWE.

Supplementary Table 1. Fitted EIS parameters of the catalysts

Sample	R_s (Ω)	R_{ct} (Ω)	CPE-T ($F \cdot s^{n-1}$)	CPE-P (n)
M4Zn-S	7.7	52.4	0.0040	0.70
M4-S	7.5	63.0	0.0043	0.75

Supplementary Table 2. Comparison of OER performance among some reported catalysts in alkaline media.

Catalysts	**3E[a]: η_{10}[b] (mV)**	**3E: η_{100}[b] (mV)**	**3E: Tafel slope[c] (mV dec^{-1})**	**3E: Durability**	**2E[d]: Durability**	**2E: Cell voltage**	**Ref.**
M4Zn-S	207	262	47.6	10–250 mA cm^{-2}, 200 h	500 mA cm^{-2}, 200 h	1.68 V@1000 mA cm^{-2}, 80 ^{o}C	This work
$FeCoNiCrMnS_x$	200	—	40.5	100 mA cm^{-2}, 100 h	—	—	1
$CoNi_2S_4$@ReS_2/ CC	253	—	54.7	—	100 mA cm^{-2}, 60 h	1.74 V@100 mA cm^{-2}, RT	2
MoZnFeCoNi	221	—	48.78	—	100 mA cm^{-2}, 1500 h	—	3
(FeCoNiCrCuAl) S@La-HCS	246	297	51.75	100 mA cm^{-2}, 60 h	—	—	4
$(NiCoFeMoIn)_3S_4$	217	254	30.1	100 mA cm^{-2}, 300 h	—	—	5
$FeCoS_y$/NCDs-3	284	—	52.1	10 mA cm^{-2}, 24 h	—	—	6
$(NiFeCoMn)_3S_4$	289	—	75.6	10 mA cm^{-2}, 48 h	—	—	7
Ni-CoS/NC	270	350	37	50 mA cm^{-2}, 300 h	—	—	8

Co_3S_4/FeS@CoFe/NC	260	—	45.34	—	10 mA cm^{-2}, 210 h	1.34 V@5 mA cm^{-2}, RT	9
$NiFeVS_x$@NF	259	377	34	10 mA cm^{-2}, 55 h	10 mA cm^{-2}, 55 h	1.60 V@10 mA cm^{-2}, RT	10
(FeCoNiCrCuAl)S	253	324	61.51	20 mA cm^{-2}, 20 h	—	—	11
$(MnFeCoNiCu)S_2$	221	—	54.4	10 mA cm^{-2}, 12 h	—	—	12
CoZnCdCuMnS@CF	220	289	64.9	10 mA cm^{-2}, 113 h	10 mA cm^{-2}, 73 h	1.63 V@10 mA cm^{-2}, RT	13
H-FeCoS/NC-0.50	240	340	81.3	10 mA cm^{-2}, 30 h	10 mA cm^{-2}, 1000 h	1.52 V@10 mA cm^{-2}, RT	14
NCOSH	243	—	63	10 mA cm^{-2}, 80 h	—	—	15

[a]3E: three-electrode system.

[b]η_{10} and η_{100}: overpotential at 10 and 100 mA cm^{-2}, respectively.

[c]Tafel slope: derived from the three–electrode LSV measurements.

[d]2E: two-electrode electrolyzer (including AEMWE).

REFERENCES

1. Cai, H. Z.; He, S. Z.; Yang, H. P.; et al. Highly exposed ultra-small high-entropy sulfides with d-p orbital hybridization for efficient oxygen evolution. *Adv. Mater.* **2025**, *37*, 2508610.[DOI:10.1002/adma.202508610]

2. Lu, Y. H.; Zhao, Z. Q.; Liu, X. T.; et al. Interface-driven catalytic enhancements in nitrogen-doped carbon immobilized $CoNi_2S_4$@ReS_2/CC heterostructures for optimized hydrogen and oxygen evolution in alkaline seawater-splitting. *Adv. Sci.* **2025**, *12*, 2413245.[DOI:10.1002/advs.202413245]

3. Mei, Y. J.; Chen, J. L.; Wang, Q.; et al. MoZn-based high entropy alloy catalysts enabled dual activation and stabilization in alkaline oxygen evolution. *Sci. Adv.* **2024**, *10*, eadq6758.[DOI:10.1126/sciadv.adq6758]

4. Wan, Y.; Wei, W. R.; Li, L.; Wu, L.; Qin, H. Y.; Yuan, X. X. Modulating support effect in high-entropy sulfide via La single-atom for boosted oxygen evolution. *Small* **2025**, *21*, 2502039.[DOI:10.1002/smll.202502039]

5. Li, Y. P.; Li, W. W.; Kou, Y. Z.; et al. Non-determining step matters: unveiling the synergistic mechanism of high-entropy $(NiCoFeMoIn)_3S_4$ catalysts for enhanced oxygen production in seawater. *Adv. Funct. Mater.* **2025**, *35*, 2422549.[DOI:10.1002/adfm.202422549]

6. Wu, L.; Qin, H. L.; Ji, Z. Y.; et al. Nitrogen-doped carbon dots modified Fe–Co sulfide nanosheets as high-efficiency electrocatalysts toward oxygen evolution reaction. *Small* **2024**, *20*, 2305965.[DOI:10.1002/smll.202305965]

7. Wu, L.; Shen, X. P.; Ji, Z. Y.; et al. Facile synthesis of medium-entropy metal sulfides as high-efficiency electrocatalysts toward oxygen evolution reaction. *Adv. Funct. Mater.* **2023**, *33*, 2208170.[DOI:10.1002/adfm.202208170]

8. Wan, K.; Luo, J. S.; Liu, W. B.; et al. Metal-organic framework-derived cation regulation of metal sulfides for enhanced oxygen evolution activity. *Chinese J. Catal.* **2023**, *54*, 290-7.[DOI:10.1016/s1872-2067(23)64533-4]

9. Tan, Y.; Wang, Y. J.; Li, A. S.; Jiang, X. C.; Zhang, Y. Z.; Cheng, C. W. Superhydrophobic Co/Fe sulfide nanoparticles and single-atoms doped carbon

nanosheets composite air cathode for high-performance zinc-air batteries. *J. Energy Chem.* **2024**, *96*, 568-77.[DOI:10.1016/j.jechem.2024.05.013]

10. He, Y. J.; Shen, J.; Li, Q.; et al. In-situ growth of VS4 nanorods on Ni-Fe sulfides nanoplate array towards achieving a highly efficient and bifunctional electrocatalyst for total water splitting. *Chem. Eng. J.* **2023**, *474*, 145461.[DOI:10.1016/j.cej.2023.145461]

11. Wan, Y.; Wei, W. R.; Ding, S. Q.; Wu, L.; Yuan, X, X. Achieving efficient oxygen evolution on high-entropy sulfide utilizing low electronegativity of Al. *Small* **2024**, *20*, 2404689.[DOI:10.1002/smll.202404689]

12. Li, F. Q.; Ma, Y. J.; Wu, H.;et al. Sub-3-nm high-entropy metal sulfide nanoparticles with synergistic effects as promising electrocatalysts for enhanced oxygen evolution reaction. *J. Phys. Chem. C* **2022**, *126*, 18323-32.[DOI:10.1021/acs.jpcc.2c05666]

13. Lei, Y. T.; Zhang, L. L.; Xu, W. J; et al. Carbon-supported high-entropy Co-Zn-Cd-Cu-Mn sulfide nanoarrays promise high-performance overall water splitting. *Nano Res.* **2022**, *15*, 6054-61.[DOI:10.1007/s12274-022-4304-8]

14. Li, X. X.; Zhang, M. Y.; Liu, Y. J; et al. Highly efficient and durable water electrolysis via ligand modulated interfacial assembly. *Appl. Catal. B Environ. Energy* **2024**, *359*, 124530.[DOI:10.1016/j.apcatb.2024.124530]

15. Zheng, X. R.; Cao, Y. H.; Wu, Z.; et al. Rational design and spontaneous sulfurization of NiCo-(oxy)hydroxysulfides nanosheets with modulated local electronic configuration for enhancing oxygen electrocatalysis. *Adv. Energy Mater.* **2022**, *12*, 2103275.[DOI:10.1002/aenm.202103275]